Size-dependent Thermal Shifts to MOF Nanocrystal Optical Gaps Induced by Dynamic Bonding

Kevin Fabrizio and Carl K. Brozek*

Department of Chemistry and Biochemistry, Material Science Institute,

University of Oregon, Eugene, OR 97403

Email: cbrozek@uoregon.edu

Abstract. Conventional semiconductor nanocrystals exhibit wide-ranging optical behavior, whereas the size-dependent photophysical properties of metal-organic framework (MOF) nanocrystals remains an open research frontier. Here, we present size- and temperature-dependent optical absorption spectra of common MOFs with particle sizes ranging from tens of nanometers to several microns. All materials exhibit optical gaps that decrease at elevated temperatures, which we attribute to the dynamic nature of MOF metal-linker bonds. Accordingly, whereas the labile titanium-carboxylate bonds of MIL-125 give rise to bandgaps that redshift by ~600 meV over 300 K, the more rigid zinc-imidazolate bonds of ZIF-8 produce a redshift of only ~10 meV. Furthermore, smaller particles induce far larger decreases to optical gaps. Taken together, these results suggest MOF bonding becomes more flexible with smaller nanocrystal sizes, offering a powerful tool for manipulating optical behavior through composition, temperature, and dimensionality.

Introduction

Optical gaps define the light needed to drive photocatalysis, photovoltaics, photoconductivity, and other optical properties by dictating the minimum energy required to photogenerate an electron-hole pair. Controlling these energies therefore permits thermodynamic optimization of wide-ranging optical processes, from charge transport across semiconductor junctions,[1–3] to product selectivity in photoredox catalysis.[4] Manipulating optical absorption is often achieved through doping, core-shell structures, cation exchange, or simply synthesizing new compositions of commonly studied materials. For example, bulk CdSe exhibits an optical gap of 1.7 eV compared to bulk HgSe, which possesses no optical gap and rather, semimetal-like behavior.[5,6] Over 100,000 distinct structure types of metal-organic frameworks (MOFs) have been

Scheme 1: Representation of MOF metal-carboxylate linkages in "loose" and "tight" configurations.

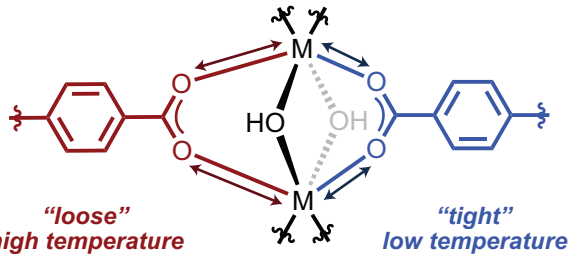

reported with a wide range of topologies, metal ions, and organic linkers, offering an extensive platform for studying the relationship between structure and optical absorption.[7–15] Rather than prepare entirely new materials, we demonstrated previously that adsorption of redox-inactive metal ions to MOF clusters causes optical gaps to shift by modulating orbital energies.[16] Whereas these techniques still require chemical modification, albeit through post-synthetic methods, external stimuli, such as heat or pressure, could offer contactless methods for controlling MOF optical behavior.

Prior work from our lab has shown that the metal-linker bonds of MOFs exist in a dynamic equilibrium between tightly and loosely bound states (**Scheme 1**).[16–18] These flexible bonds can trigger phase changes in MOFs by serving as "soft modes," and help to explain important MOF behavior, ranging from MOF crystal growth mechanisms and post-synthetic exchange to catalysis and MOF melting. As equilibrium species, we expect these bonds to respond to external stimuli because metal ions and linkers dominate frontier orbitals, and because the strength of metal-linker interactions dictate orbital energies. We therefore anticipate MOF optical behavior that can be tuned by altering the equilibrium of metal-linker tight and loose bond configurations.

Particle size offers another important parameter for controlling optical properties without altering the atomic composition of a material. By preparing a semiconductor smaller than its excitonic Bohr radius, the electronic structure undergoes quantum confinement: the electronic bands become discretized into orbitals separated by tens-to-hundreds of millielectronvolts, and the

optical absorption and photoluminescence bands narrow and blueshift with smaller particle sizes.[19] Due to the insulating nature of most MOFs, however, quantum confinement is unlikely to occur in MOF nanoparticles (nanoMOFs). Recently, we demonstrated that the semiconductor MOF Fe(1,2,3-triazolate)$_2$ can be prepared as sizes ranging from hundreds of nanometers to six nanometers—the smallest nanoMOF prepared to-date.[20] These synthetic methods leveraged previous insights into a "seesaw model" of MOF growth that relies on the presence of a molecular additive termed a "modulator".[21,22] Surprisingly, the optical absorption profiles of these nanoMOFs blueshift relative to the bulk spectrum of Fe(1,2,3-triazolate)$_2$ by as much as ~200 meV, even for particles as large as ~120 nm. For quantum confinement to cause these size-dependent optical shifts, the excitonic Bohr radius would need to be similarly large, i.e., at least ~120 nm. This explanation is unlikely given that conventional semiconductors exhibit Bohr radii smaller than 10 nm. While this phenomenon remains actively studied, we surmise that the higher surface-to-volume ratios of smaller particles play an important role in controlling the nanoMOF electronic structure. Despite these promising investigations, the impact of particle size on MOF optical properties remains an open research frontier.

Here, we demonstrate that the optical gaps of common MOFs decrease by hundreds of millielectronvolts at temperatures far below MOF decomposition, in stark contrast to the behavior of conventional semiconductors. Additionally, this temperature response depends strongly on MOF particle sizes, suggesting MOF metal-linker bonds become more flexible with smaller crystallites. These results illustrate the utility of harnessing labile metal-ligand bonds—the basic building block of inorganic structure-function relations—in achieving unprecedent size- and stimuli-dependent properties.

Results and Discussion

To understand the impact of particle size and dynamic bonding on the optical properties of MOFs, we targeted $Ti_8O_8(OH)_4$(terephthalate)$_6$ (MIL-125) due to its frequent use as a sensitizer for photoredox reactivity and because seminal reports of MOF optical properties were first demonstrated with it and related derivatives, such as $Ti_8O_8(OH)_4$(2-amino-terephthalate)$_6$ (MIL-125- NH_2). Following our recently reported reflux-based synthesis,[23] three batches of MIL-125 nanoparticles were prepared with particle sizes controlled by varying the equivalents of benzoic acid, as a modulator, relative to the amount of $Ti(OBu)_4$ precursor (see Supporting Information). Phase purity was verified by PXRD analysis (**Fig. S1-3**) and sizes were determined by SEM (**Fig. S4-12**). Based on statistical analysis of the SEM images, the resulting batches exhibited averages sizes of 79±18 nm, 215±19 nm, 424±249 nm with dispersity indices of 0.23, 0.32, and 0.59, respectively.

To probe the impact of thermal energy on the optical absorption of MIL-125 nanoMOFs, variable-temperature diffuse-reflectance UV-vis spectra were collected on powder samples of each of the three sizes. **Figure 1** shows the resulting spectra of the materials kept under dynamic vacuum and analyzed between 163 and 523 K. Qualitatively, all three samples exhibit dramatic changes to

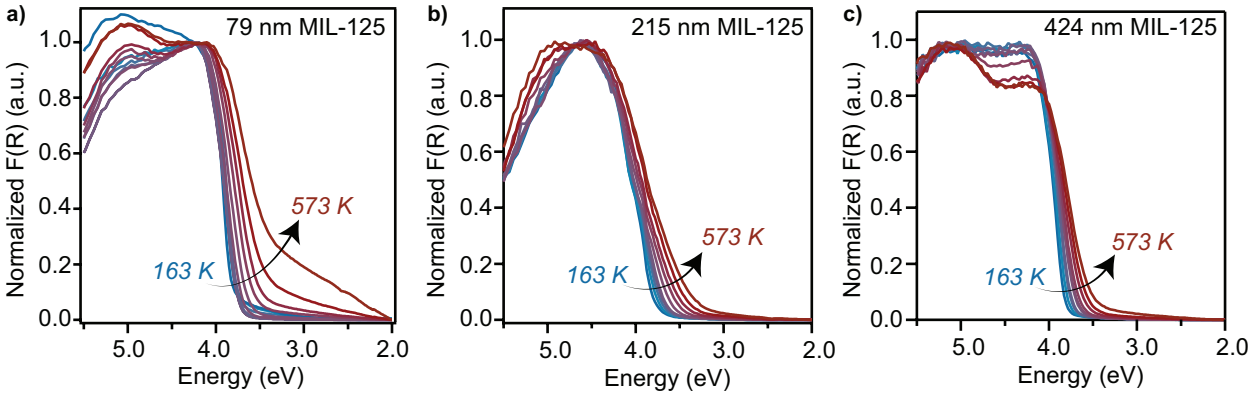

Figure 1: Variable-temperature diffuse reflectance UV-vis spectra of MIL-125 nanoparticles with diameters a) 79 nm b) 215 nm, and c) 424 nm. All samples were evacuated at room temperature and cooled to 163 K. Spectra correspond to 25 K increments between 163 – 298 K, and 50 K increments between 298 and 573 K.

their absorption profiles with several distinct features: 1) higher temperatures induce the formation of low-energy absorption tails; 2) higher temperatures causes the low-energy peak maxima to redshift; and 3) higher temperatures cause an inversion of the relative intensities of high-energy charge-transfer bands. By contrast, the optical gaps of conventional semiconductors, such as Si and InP, also redshift, but to a much lesser degree.[24] For example, the optical gap of InAs redshifts by ~80 meV over a 300 K range, whereas the onset absorption of 79-nm MIL-125 particles at 573 K appears nearly ~2.0 eV below the onset at 163 K. Variable temperature absorption spectra of TiO_2 were collected to investigate the accuracy of these shifts. Consistent with previous reports, a shift of just 60 meV was found between low and high temperatures (**Figure S20)**. These temperature-induced absorption tails were observed previously for bulk crystals of the family of MOFs known as $Ti_3M_3(\mu_3\text{-}O)_2$(1,3,5-benzenetricarboxylate)$_4$ (M = Ca, Sr, Ba, Cd) (MUV-10). This effect was ascribed to the loose-tight bonding equilibrium of MOFs causing reversible changes to the frontier orbitals.[16] This microscopic explanation of dynamic bonding in MOFs is analogous to the cause of thermal shifts in conventional semiconductors, where higher temperatures weaken the orbital overlap between adjacent atoms, causing orbital splittings to diminish.[25] But whereas the absorption redshifts in semiconductors arise from expansions of lattice constants, the thermal shifts observed for MUV-10 were attributed to thermally induced, albeit reversible, geometric rearrangements. In other words, thermal shifts in conventional semiconductors retain the electronic symmetry of the material, whereas thermal shifts in MOFs involve more severe geometric distortions. This microscopic picture would explain the features in **Fig. 1** because such distortions generate 1) "midgap" orbitals, producing the absorption tails, 2) the rigid shifts to absorption maximum through lattice expansion, and 3) changes to high-energy absorption bands through symmetry-lowered electronic structures.

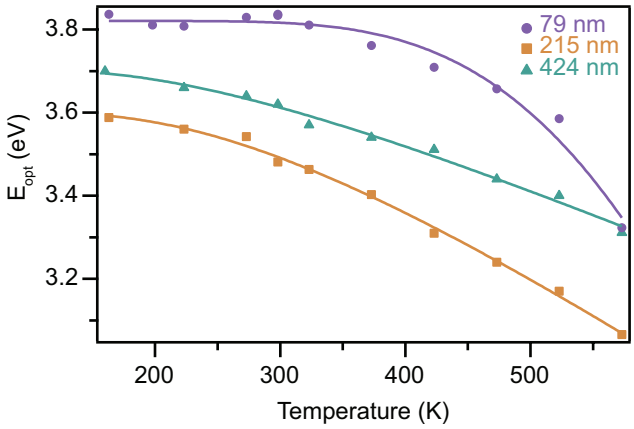

Figure 2: Optical gaps of MIL-125 nanoparticles plotted versus temperature. Solid lines represent fits based on the O'Donnell and Chen model described in Ref. 8.

While all sizes show temperature-dependent absorption profiles, smaller particles exhibit far greater sensitivity to temperature. To understand these size- and temperature-dependent spectral shifts, we sought a model that would provide a microscopic explanation. Seminal studies of temperature-dependent optical gaps were pioneered by Varshni and the phenomenon has since been termed the "Varshni effect" in semiconductors.[24] Although the model developed by Varshni remains in use for quantifying aspects of the temperature dependence, the fitted parameters lack a clear physical meaning. Therefore, we employed an alternative model pioneered by O'Donnell and Chen that employs parameters related to bonding and vibronic interactions (**Eq. 1**).[26]

$$E_{opt}(T) = E_0 - S\langle\hbar\omega\rangle[\coth(\langle\hbar\omega\rangle/2kT) - 1] \qquad \textbf{Eq.1}$$

To determine the optical gaps (E_{opt}), the spectra in **Fig. 1** were fitted through Tauc analysis. Recently, we evaluated different methods of determining MOF optical gaps and endorsed the Tauc analysis only for MOFs with overlapping optical bands, typically resulting from ligand field transitions or midgap states.[27] Although Gaussian fitting is appropriate for analyzing the MIL-125 spectra at low temperatures where optical bands are clearly distinguishable, Tauc analysis is best suited for the pronounced absorption tails at higher temperatures. **Figure 2** plots the resulting E_{opt} for the 79 nm, 215 nm, and 424 nm particles across all temperatures. Due to the uncertainty

Scheme 2: Representation of the relationship of Huang-Rhys parameter S to equilibrium nuclear positions (ΔQ_i).

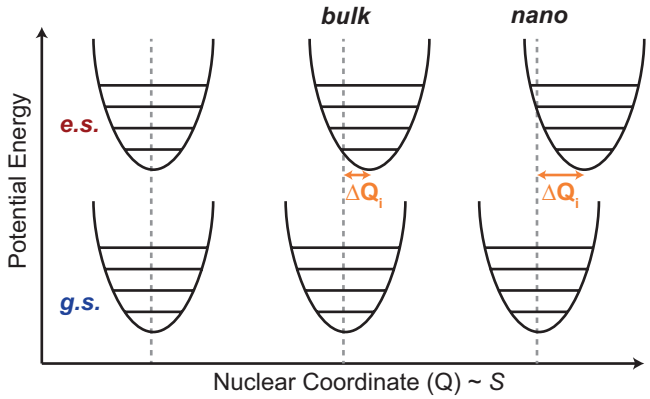

inherent in determining E_{opt} by Tauc analysis, we place greater emphasis on temperature-dependence of the values rather than the absolute energies. Fitting these data to the O'Donnell and Chen model produced excellent fits displayed as solid lines in **Fig. 2**. As seen in the curvature of the fits, and as reflected qualitatively in **Fig. 1**, the smaller particles exhibit the greatest sensitivity to temperature. In this model, E_0 denotes the 0-K E_{opt}, S represents the Huang-Rhys parameter, and $\langle\hbar\omega\rangle$ gives the average phonon energy. Chemically, S is a unit-less measure of vibronic coupling and is proportional to the offset in the equilibrium nuclear positions (ΔQ_i) between ground and excited state geometries (**Scheme 2**).[28] For typical molecules and semiconductors $S < 10$, while for ionic solids $S > 50$. Therefore, both $\langle\hbar\omega\rangle$ and S indicate the structural flexibility of material because large $\langle\hbar\omega\rangle$ implies many vibrational states can be activated at a given temperature, while a large S implies strong vibronic distortions. **Table 1** summarizes the fitting results. Because S dominates the slope of the fit, according to the O'Donnell and Chen model, an inverse relationship between nanoMOF size and S is evident from the data in **Fig. 2**. Clearly, the unusually large S values for 79-nm MIL-125 nanoparticles suggest MOF bonding becomes more dynamic with smaller crystallites.

Table 1: Fit parameters derived from fitting temperature-dependent optical gaps for MIL-125, UiO-66, and ZIF-8 nanoparticles to the O'Donnell and Chen Model. E_0, S, and $\langle \hbar\omega \rangle$ denote the zero-temperature optical gap, Huang-Rhys parameter, and average phonon energy, respectively.

	MIL-125			**UiO-66**			**ZIF-8**		
Size (nm)	79	215	424	26	105	4050	49	205	1000
E_0 (eV)	3.82	3.60	3.70	4.12	4.47	4.11	5.30	5.32	5.28
S	89.5	12.7	7.82	11.9	3.45	2.53	0.83	0.59	2.83
$\langle \hbar\omega \rangle$ (eV)	0.221	0.075	0.064	0.089	0.078	0.033	0.048	-0.002	0.055

To explore the generality of these size-dependent thermal shifts and their relation to metal-linker bonding, variable-temperature diffuse-reflectance UV-vis spectra were collected on nanoparticles of two distinct classes of MOF materials. Considered among the most stable MOFs, $Zr_6O_4(OH)_4$(terephthalate)$_{12}$ (UiO-66) and Zn(2-methylimidazolate)$_2$ (ZIF-8) should display less dynamic metal-linker bonding than MIL-125. Additionally, they offer a useful comparison because MIL-125 and UiO-66 have similar metal bonding environments and because ZIF-8 is comprised of metal-azolate, rather than carboxylate, linkages. Following previous reports, 26±3.2 nm, 105±19 nm, and 4.05±0.27 μm (bulk) particles were prepared for UiO-66 and 49±9.7 nm, 205±9.8 nm, and 2.35±0.45 μm (bulk) particles were prepared for ZIF-8 (see Supporting Information).[29–32] **Figures S16 and S17** show that the resulting spectra of UiO-66 and ZIF-8 collected under similar conditions to MIL-125. Qualitatively, UiO-66 exhibits greater size- and temperature-dependence than ZIF-8, but less than MIL-125. **Table 1** summarizes fits of the E_{opt} values to the O'Donnell and Chen model. Like MIL-125, smaller particles of UiO-66 show larger S and $\langle \hbar\omega \rangle$. The smaller absolute values of these parameters corroborates UiO-66 being considered among the most water- and pH-stable MOFs.[33] By comparison, the E_{opt} of bulk and nanosized ZIF-8 show little sensitivity to temperature or size, suggesting greater rigidity of the Zn-imidazolate bonds. To

compare the temperature- and size-dependent thermal shifts of all three MOFs, **Figure 3** plots difference spectra defined as the difference between *F(R)* collected at 473 K and 163 K for each of the bulk and smallest nanoMOF samples. Therefore, positive intensity corresponds to increased absorption at higher temperatures. Inspection of **Fig. 1**, **S16, and S17** suggest that the well-defined bands in **Fig. 3** between 3.0 – 4.0 eV correspond to redshifts to the original HOMO-LUMO absorption profiles, whereas the positive intensity observed between 2.0 – 3.5 eV correspond to the formation of midgap states. Between all samples, MIL-125 showed the largest increase in redshifted band-edge (HOMO-LUMO) absorption. The inset of **Fig. 3** compares the normalized differential absorption onsets between UiO-66 and MIL-125. Interestingly, the nanoparticles of UiO-66 displayed a greater redshift relative to the bulk spectra in comparison to the redshifts of MIL-125. These results suggest that size reduction causes a greater thermal redshift in the band-edge absorption for UiO-66 compared to MIL-125. On the other hand, the main effect of size reduction of MIL-125 is the thermally induced creation of midgap states. For ZIF-8, nanoparticles showed a greater temperature dependence than the bulk material, overall, with a minor increase in

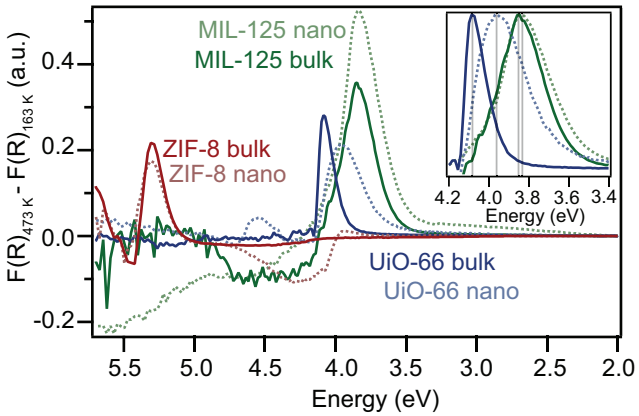

Figure 3: Temperature-differential UV-vis spectra for bulk and nano-sized MOFs defined as the difference in the Kubelka-Munk functions F(R) recorded at 473 K and 163 K for each material. Data for Zif-8, MIL-125, and UiO-66 are shown in red, green, and blue, respectively. 50 and 2000 nm ZIF-8, 79 and 424 nm MIL-125, and 26 and 4050 nm UiO-66 were used. Inset: Normalized differential absorption for UiO-66 and MIL-125.

absorption intensity near the band-edge around ~4.0 eV, but differences were less pronounced in comparison to MIL-125 and UiO-66.

These results for MOF nanocrystals represent an extreme example of temperature- and size-dependent optical behavior observed previously for quantum-confined semiconductor nanocrystals (quantum dots). For example, fitting E_{opt} data for CdTe quantum dots to the O'Donnell and Chen model showed that decreasing particle sizes from 3.6 nm to 2.6 nm caused an increase in S from 1.9 to 2.4 and an increase in $\langle \hbar\omega \rangle$ from 12.3 meV to 12.7 meV.[34] This phenomenon has been widely observed for quantum dots and has been attributed to enhanced

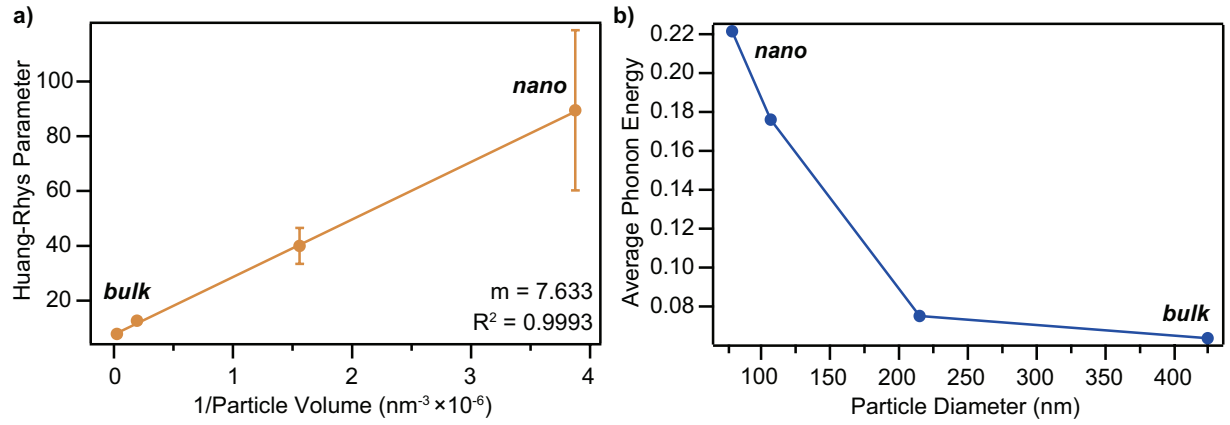

Figure 4: Huang-Rhys parameters and average phonon energies derived for various MIL-125 plotted against inverse particle volumes and particle diameters, respectively.

exciton-phonon interactions in smaller crystallite sizes.[35] Furthermore, theoretical analysis predicts S to be proportional to a^3/V, where a represents the Bohr radius and V the particle volume. Although quantum confinement is unlikely for MOF particles of these sizes, we explored whether the size-dependence of electron-phonon interactions in MIL-125 nanoparticles, S, relates to changes in nanoMOF volumes. Indeed, **Fig. 4a** and **S20** show a remarkable correlation between S for MIL-125 and UiO-66 nanoparticles versus inverse particle volumes. We propose that this linear relationship arises from changes to the nature of metal-linker bonding with decreased crystallite sizes, as has been observed in other classes of nanocrystals lacking quantum

confinement effects. For example, lattice parameters of metal oxide nanocrystals generally increase in smaller particles. This effect has been ascribed to weaker Madelung fields that create a "negative pressure". In other words, large surface-to-volume ratios decrease the electrostatic stabilization that holds the particles intact and thereby bonding weakens.[36] Similarly, smaller alumina nanoparticles become more compressible[37], and Si nanocrystals exhibit lower melting point temperatures and smaller bulk moduli.[38] The smaller slope for UiO-66 would therefore imply less flexible bonding compared to MIL-125, further support that UiO-66 is among the most stable MOFs. In conjunction with Huang-Rhys parameter, **Figure 4b** highlights the significant increase in average phonon energy as particle diameter decreases in MIL-125. These results highlight an increase in overall lattice vibration frequency, as previously observed in semiconductor nanoparticles.[39] Taken together, these results suggest that the optical absorption of smaller MOF particles display greater temperature dependence due to enhanced bond flexibility.

Conclusion

This experimental study shows that the optical gaps of the common MOFs MIL-125, UiO-66, and ZIF-8 decrease at elevated temperatures to a far greater degree than conventional semiconductors and that this effect becomes magnified for smaller nanoparticle sizes. Whereas MIL-125 exhibits the greatest sensitivity, ZIF-8 shows the least. Given that UiO-66 and ZIF-8 are considered the among the most stable MOFs, these results suggest a relationship between optical gap thermal shifts to bonding strength. Based on fitting the temperature-dependent optical gaps to a model based on vibronic coupling, these results suggest that MOF metal-linker bonding becomes more dynamic and flexible with smaller particle sizes, allowing control over optical behavior difficult to achieve with other classes of molecules and materials.

Acknowledgements

This material is based upon work supported by the Department of Energy through the Office of Basic Energy Sciences under grant no. DE-SC0022147. C.K.B. acknowledges the Research Corporation for Science Advancement (Cottrell Award).

References

(1) Kamat, P. V. Manipulation of Charge Transfer Across Semiconductor Interface. A Criterion That Cannot Be Ignored in Photocatalyst Design. *J. Phys. Chem. Lett.* **2012**, *3* (5), 663–672. https://doi.org/10.1021/jz201629p.

(2) Chen, M.; Dong, H.; Xue, M.; Yang, C.; Wang, P.; Yang, Y.; Zhu, H.; Wu, C.; Yao, Y.; Luo, W.; Zou, Z. Faradaic Junction and Isoenergetic Charge Transfer Mechanism on Semiconductor/Semiconductor Interfaces. *Nat. Commun.* **2021**, *12* (1), 6363. https://doi.org/10.1038/s41467-021-26661-6.

(3) Tvrdy, K.; Frantsuzov, P. A.; Kamat, P. V. Photoinduced Electron Transfer from Semiconductor Quantum Dots to Metal Oxide Nanoparticles. *Proc. Natl. Acad. Sci.* **2011**, *108* (1), 29–34. https://doi.org/10.1073/pnas.1011972107.

(4) Yang, K.; Yang, Z.; Zhang, C.; Gu, Y.; Wei, J.; Li, Z.; Ma, C.; Yang, X.; Song, K.; Li, Y.; Fang, Q.; Zhou, J. Recent Advances in CdS-Based Photocatalysts for CO_2 Photocatalytic Conversion. *Chem. Eng. J.* **2021**, *418*, 129344. https://doi.org/10.1016/j.cej.2021.129344.

(5) Soloviev, V. N.; Eichhöfer, A.; Fenske, D.; Banin, U. Molecular Limit of a Bulk Semiconductor: Size Dependence of the "Band Gap" in CdSe Cluster Molecules. *J. Am. Chem. Soc.* **2000**, *122* (11), 2673–2674. https://doi.org/10.1021/ja9940367.

(6) Harman, T. C.; Strauss, A. J. Band Structure of HgSe and HgSe–HgTe Alloys. *J. Appl. Phys.* **1961**, *32* (10), 2265–2270. https://doi.org/10.1063/1.1777057.

(7) Shustova, N. B.; Cozzolino, A. F.; Reineke, S.; Baldo, M.; Dincă, M. Selective Turn-On Ammonia Sensing Enabled by High-Temperature Fluorescence in Metal–Organic Frameworks with Open Metal Sites. *J. Am. Chem. Soc.* **2013**, *135* (36), 13326–13329. https://doi.org/10.1021/ja407778a.

(8) Dolgopolova, E. A.; Rice, A. M.; Martin, C. R.; Shustova, N. B. Photochemistry and Photophysics of MOFs: Steps towards MOF-Based Sensing Enhancements. *Chem. Soc. Rev.* **2018**, *47* (13), 4710–4728. https://doi.org/10.1039/C7CS00861A.

(9) Son, H.-J.; Jin, S.; Patwardhan, S.; Wezenberg, S. J.; Jeong, N. C.; So, M.; Wilmer, C. E.; Sarjeant, A. A.; Schatz, G. C.; Snurr, R. Q.; Farha, O. K.; Wiederrecht, G. P.; Hupp, J. T. Light-Harvesting and Ultrafast Energy Migration in Porphyrin-Based Metal–Organic Frameworks. *J. Am. Chem. Soc.* **2013**, *135* (2), 862–869. https://doi.org/10.1021/ja310596a.

(10) Martin, C. R.; Leith, G. A.; Kittikhunnatham, P.; Park, K. C.; Ejegbavwo, O. A.; Mathur, A.; Callahan, C. R.; Desmond, S. L.; Keener, M. R.; Ahmed, F.; Pandey, S.; Smith, M. D.; Phillpot, S. R.; Greytak, A. B.; Shustova, N. B. Heterometallic Actinide-Containing Photoresponsive Metal-Organic Frameworks: Dynamic and Static Tuning of Electronic Properties. *Angew. Chem. Int. Ed.* **2021**, *60* (15), 8072–8080. https://doi.org/10.1002/anie.202016826.

(11) Castells-Gil, J.; Padial, N. M.; Almora-Barrios, N.; Albero, J.; Ruiz-Salvador, A. R.; González-Platas, J.; García, H.; Martí-Gastaldo, C. Chemical Engineering of Photoactivity in

Heterometallic Titanium–Organic Frameworks by Metal Doping. *Angew. Chem. Int. Ed.* **2018**, *57* (28), 8453–8457. https://doi.org/har.
(12) Cornell, H. D.; Zhu, Y.; Ilic, S.; Lidman, N. E.; Yang, X.; Matson, J. B.; Morris, A. J. Green-Light-Responsive Metal–Organic Frameworks for Colorectal Cancer Treatment. *Chem. Commun.* **2022**, *58* (34), 5225–5228. https://doi.org/10.1039/D2CC00591C.
(13) Nguyen, H. L.; Gándara, F.; Furukawa, H.; Doan, T. L. H.; Cordova, K. E.; Yaghi, O. M. A Titanium–Organic Framework as an Exemplar of Combining the Chemistry of Metal– and Covalent–Organic Frameworks. *J. Am. Chem. Soc.* **2016**, *138* (13), 4330–4333. https://doi.org/10.1021/jacs.6b01233.
(14) Shen, L.; Liang, S.; Wu, W.; Liang, R.; Wu, L. Multifunctional NH_2-Mediated Zirconium Metal–Organic Framework as an Efficient Visible-Light-Driven Photocatalyst for Selective Oxidation of Alcohols and Reduction of Aqueous Cr(VI). *Dalton Trans.* **2013**, *42* (37), 13649–13657. https://doi.org/10.1039/C3DT51479J.
(15) Maza, W. A.; Morris, A. J. Photophysical Characterization of a Ruthenium(II) Tris(2,2′-Bipyridine)-Doped Zirconium UiO-67 Metal–Organic Framework. *J. Phys. Chem. C* **2014**, *118* (17), 8803–8817. https://doi.org/10.1021/jp501140r.
(16) Fabrizio, K.; Lazarou, K. A.; Payne, L. I.; Twight, L. P.; Golledge, S.; Hendon, C. H.; Brozek, C. K. Tunable Band Gaps in MUV-10(M): A Family of Photoredox-Active MOFs with Earth-Abundant Open Metal Sites. *J. Am. Chem. Soc.* **2021**, *143* (32), 12609–12621. https://doi.org/10.1021/jacs.1c04808.
(17) Andreeva, A. B.; Le, K. N.; Chen, L.; Kellman, M. E.; Hendon, C. H.; Brozek, C. K. Soft Mode Metal-Linker Dynamics in Carboxylate MOFs Evidenced by Variable-Temperature Infrared Spectroscopy. *J. Am. Chem. Soc.* **2020**, *142* (45), 19291–19299. https://doi.org/10.1021/jacs.0c09499.
(18) Andreeva, A. B.; Le, K. N.; Kadota, K.; Horike, S.; Hendon, C. H.; Brozek, C. K. Cooperativity and Metal–Linker Dynamics in Spin Crossover Framework Fe(1,2,3-Triazolate)$_2$. *Chem. Mater.* **2021**, *33* (21), 8534–8545. https://doi.org/10.1021/acs.chemmater.1c03143.
(19) Murray, C. B.; Norris, D. J.; Bawendi, M. G. Synthesis and Characterization of Nearly Monodisperse CdE (E = Sulfur, Selenium, Tellurium) Semiconductor Nanocrystallites. *J. Am. Chem. Soc.* **1993**, *115* (19), 8706–8715. https://doi.org/10.1021/ja00072a025.
(20) Marshall, C. R.; Dvorak, J. P.; Twight, L. P.; Chen, L.; Kadota, K.; Andreeva, A. B.; Overland, A. E.; Ericson, T.; Cozzolino, A. F.; Brozek, C. K. Size-Dependent Properties of Solution-Processable Conductive MOF Nanocrystals. *J. Am. Chem. Soc.* **2022**. https://doi.org/10.1021/jacs.1c10800.
(21) Marshall, C. R.; Staudhammer, S. A.; Brozek, C. K. Size Control over Metal–Organic Framework Porous Nanocrystals. *Chem. Sci.* **2019**, *10* (41), 9396–9408. https://doi.org/10.1039/C9SC03802G.
(22) Marshall, C. R.; Timmel, E. E.; Staudhammer, S. A.; Brozek, C. K. Experimental Evidence for a General Model of Modulated MOF Nanoparticle Growth. *Chem. Sci.* **2020**, *11* (42), 11539–11547. https://doi.org/10.1039/d0sc04845c.
(23) Fabrizio, K.; Brozek, C. Photoredox-Active Colloids and Polymer Membranes of Titanium-Based MOF Nanoparticles. **2022**. https://doi.org/10.26434/chemrxiv-2022-knxwb.
(24) Varshni, Y. P. Temperature Dependence of the Energy Gap in Semiconductors. *Physica* **1967**, *34* (1), 149–154. https://doi.org/10.1016/0031-8914(67)90062-6.

(25) Zeier, W. G.; Zevalkink, A.; Gibbs, Z. M.; Hautier, G.; Kanatzidis, M. G.; Snyder, G. J. Thinking Like a Chemist: Intuition in Thermoelectric Materials. *Angew. Chem. Int. Ed.* **2016**, *55* (24), 6826–6841. https://doi.org/10.1002/anie.201508381.
(26) O'Donnell, K. P.; Chen, X. Temperature Dependence of Semiconductor Band Gaps. *Appl. Phys. Lett.* **1991**, *58* (25), 2924–2926. https://doi.org/10.1063/1.104723.
(27) Fabrizio, K.; Le, K. N.; Andreeva, A. B.; Hendon, C. H.; Brozek, C. K. Determining Optical Band Gaps of MOFs. *ACS Mater. Lett.* **2022**, *4* (3), 457–463. https://doi.org/10.1021/acsmaterialslett.1c00836.
(28) de Jong, M.; Seijo, L.; Meijerink, A.; Rabouw, F. T. Resolving the Ambiguity in the Relation between Stokes Shift and Huang–Rhys Parameter. *Phys. Chem. Chem. Phys.* **2015**, *17* (26), 16959–16969. https://doi.org/10.1039/C5CP02093J.
(29) Shangkum, G. Y.; Chammingkwan, P.; Trinh, D. X.; Taniike, T. Design of a Semi-Continuous Selective Layer Based on Deposition of UiO-66 Nanoparticles for Nanofiltration. *Membranes* **2018**, *8* (4), 129. https://doi.org/10.3390/membranes8040129.
(30) Katz, M. J.; Brown, Z. J.; Colón, Y. J.; Siu, P. W.; Scheidt, K. A.; Snurr, R. Q.; Hupp, J. T.; Farha, O. K. A Facile Synthesis of UiO-66, UiO-67 and Their Derivatives. *Chem. Commun.* **2013**, *49* (82), 9449–9451. https://doi.org/10.1039/C3CC46105J.
(31) Schejn, A.; Balan, L.; Falk, V.; Aranda, L.; Medjahdi, G.; Schneider, R. Controlling ZIF-8 Nano- and Microcrystal Formation and Reactivity through Zinc Salt Variations. *CrystEngComm* **2014**, *16* (21), 4493–4500. https://doi.org/10.1039/C3CE42485E.
(32) Chen, C.; Ozcan, A.; Yazaydin, A. O.; Ladewig, B. P. Gas Permeation through Single-Crystal ZIF-8 Membranes. *J. Membr. Sci.* **2019**, *575*, 209–216. https://doi.org/10.1016/j.memsci.2019.01.027.
(33) Liu, X.; Demir, N. K.; Wu, Z.; Li, K. Highly Water-Stable Zirconium Metal–Organic Framework UiO-66 Membranes Supported on Alumina Hollow Fibers for Desalination. *J. Am. Chem. Soc.* **2015**, *137* (22), 6999–7002. https://doi.org/10.1021/jacs.5b02276.
(34) Balakrishnan, J.; L K, P.; D, S.; Jagtap, A.; Madapu, K. K.; Dhara, S.; Rao, K. S. R. K. Temperature- and Size-Dependent Photoluminescence in Colloidal CdTe and $Cd_xZn_{1-x}Te$ Quantum Dots. *J. Phys. Appl. Phys.* **2021**, *54* (14), 145103. https://doi.org/10.1088/1361-6463/abd6d3.
(35) Schmitt-Rink, S.; Miller, D. A. B.; Chemla, D. S. Theory of the Linear and Nonlinear Optical Properties of Semiconductor Microcrystallites. *Phys. Rev. B* **1987**, *35* (15), 8113–8125. https://doi.org/10.1103/PhysRevB.35.8113.
(36) Perebeinos, V.; Chan, S.-W.; Zhang, F. 'Madelung Model' Prediction for Dependence of Lattice Parameter on Nanocrystal Size. *Solid State Commun.* **2002**, *123* (6), 295–297. https://doi.org/10.1016/S0038-1098(02)00266-1.
(37) Chen, B.; Penwell, D.; Benedetti, L. R.; Jeanloz, R.; Kruger, M. B. Particle-Size Effect on the Compressibility of Nanocrystalline Alumina. *Phys. Rev. B* **2002**, *66* (14), 144101. https://doi.org/10.1103/PhysRevB.66.144101.
(38) Abdullah, B. J.; Omar, M. S.; Jiang, Q. Size Dependence of the Bulk Modulus of Si Nanocrystals. *Sādhanā* **2018**, *43* (11), 174. https://doi.org/10.1007/s12046-018-0956-1.
(39) Liang, L.; Ma, H.; Wei, Y. Size-Dependent Elastic Modulus and Vibration Frequency of Nanocrystals. *J. Nanomater.* **2011**, *2011*, 670857. https://doi.org/10.1155/2011/670857.